

Quantum Criticality of Excitonic Insulating Transition in Nodal Line Semimetal ZrSiS

Jing-Rong Wang,¹ Guo-Zhu Liu,^{2,*} Xiangang Wan,^{3,4} and Changjin Zhang^{1,4,5,†}

¹Anhui Province Key Laboratory of Condensed Matter Physics at Extreme Conditions,
High Magnetic Field Laboratory of the Chinese Academy of Sciences, Hefei 230031, China

²Department of Modern Physics, University of Science and Technology of China, Hefei 230026, China

³National Laboratory of Solid State Microstructures,

College of Physics, Nanjing University, Nanjing 210093, China

⁴Collaborative Innovation Center of Advanced Microstructures, Nanjing University, Nanjing 210093, China

⁵Institutes of Physical Science and Information Technology, Anhui University, Hefei 230601, China

Pezzini *et al.* reported an unconventional mass enhancement in topological nodal line semimetal ZrSiS (Nat. Phys. **14**, 178 (2018)), whose origin remains puzzling. In this material, strong short-range interactions might induce excitonic particle-hole pairs. Here we study the renormalization of fermion velocities and find that the mass enhancement in ZrSiS can be well understood if we suppose that ZrSiS is close to the quantum critical point between semimetal and excitonic insulator. Near this quantum critical point, the fermion velocities are considerably reduced by excitonic quantum fluctuation, leading to fermion mass enhancement. The quasiparticle residue is suppressed as the energy decreases but is finite at zero energy. This indicates that ZrSiS is a strongly correlated Fermi liquid, and explains why the mass enhancement is weaker than non-Fermi liquids. Our results suggest that ZrSiS is a rare example of 3D topological semimetal exhibiting unusual quantum criticality.

Quantum phase transition has emerged as one of the most important subjects in modern condensed matter physics. For a second-order transition, thermodynamic phases with distinct symmetries are separated by a quantum critical point (QCP). In the vicinity of the QCP, the low-energy quasiparticle properties are governed by the quantum fluctuation of order parameter such that some interesting unconventional phenomena could arise, e.g., a significant enhancement or divergence of quasiparticle mass [1]. In real systems, quantum criticality exhibiting greatly enhanced mass has been observed in a variety of materials, including cuprates $\text{YBa}_2\text{Cu}_3\text{O}_{6+\delta}$ [2] and $\text{Eu}(\text{Nd})\text{-LSCO}$ [3], heavy fermion compounds YbRh_2Si_2 , CeCoIn_5 , and CeRhIn_5 [4–6], iron pnictide $\text{BaFe}(\text{As}_x\text{P}_{1-x})_2$ [7], and spinel magnet ZnCr_2Se_4 [8].

In the past decade, much efforts have been put into the topological semimetal (SM) materials [9–17]. In these SMs, most behaviors are manifested by their single-particle characters. However, under certain conditions, inter-particle interactions can markedly renormalize the energy dispersion of free fermions, and even cause quantum phase transitions [18–29]. For SMs tuned close to band-touching point, there is perfect particle-hole symmetry and the semimetallic ground state may become unstable due to particle-hole pairing [30], leading to an excitonic insulating transition. This would be a nice platform to study quantum critical phenomena in SMs, such as unusual mass enhancement. Nevertheless, excitonic instability requires a sufficiently strong long-range Coulomb interaction (LRCI) or short-range four-fermion interaction [31–35], which is not easy to realize in actual systems. Although there are many proposals for

excitonic transition in various SMs [31–36], so far experimental evidences of excitonic QCP and the associated quantum critical phenomena are still limited.

Recently, Pezzini *et al.* [37] have measured the quantum oscillations of ZrSiS, a topological nodal line SM (NLSM), and revealed an unconventional enhancement of quasiparticle mass. Similar to what happens in cuprate $\text{YBa}_2\text{Cu}_3\text{O}_{6+\delta}$ and other materials, the observed mass enhancement is conjectured [37] to be induced by electronic correlations. The physical mechanism underlying this observation is still undetermined. Numerical calculations based on a simplified two-dimensional model [34] suggested that ZrSiS may become an excitonic insulator at low temperatures due to strong short-range interaction, which opens a finite pseudogap in the electronic spectrum. However, the opening of a finite excitonic gap is in contradiction to angle-resolved photoemission spectroscopy (ARPES) [38–40] and transport [41, 42] experiments on ZrSiS. In order to resolve this puzzle, one should search for a physical mechanism that enhances the quasiparticle mass and meanwhile is not at odds with the existing ARPES and transport experiments. It is also interesting to understand why the mass enhancement of ZrSiS is not as significant as the previously mentioned unconventional superconductors [2–7].

In this Letter, we analyze the dynamics of nodal line fermions near an excitonic instability of NLSM and demonstrate that the excitonic quantum fluctuation can considerably increase the fermion mass without gapping the system. This provides a promising explanation of the unconventional mass enhancement of ZrSiS [37]. To illustrate our proposal, we plot a schematic phase diagram in Fig. 1. Tuning the parameter x drives a quantum phase transition between NLSM and excitonic insulator (EI), with x_c being the QCP. The system is gapless in SM phase ($x < x_c$), and acquires a gap in EI phase due to excitonic pairing ($x > x_c$). For ZrSiS, x can be identi-

*Corresponding author: gzliu@ustc.edu.cn

†Corresponding author: zhangcj@hmf.ac.cn

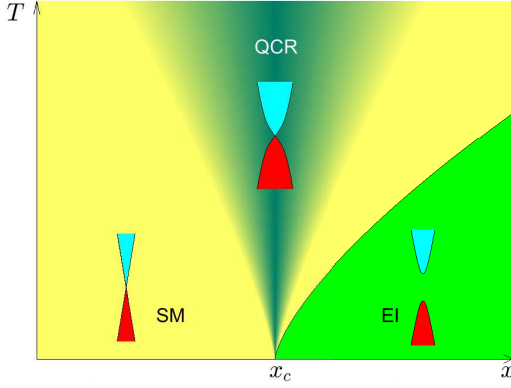


FIG. 1: Schematic global phase diagram of NLSM. Here, SM stands for semimetal, EI for excitonic insulator, and QCR for quantum critical region. SM-EI transition occurs by tuning a non-thermal parameter x , and x_c is the QCP. In QCR, the excitonic quantum fluctuation leads to considerable fermion mass enhancement.

fied as the strength parameter of short-range interaction. First of all, we infer that ZrSiS cannot be deep in the EI phase, since experiments [38–42] did not observe a finite gap. Deep in the SM phase, there are no excitonic pairs, and nodal line fermions are subjected to LRCI and weak short-range interaction. RG analysis show that, LRCI tends to reduce the mass, whereas the weak short-range interaction does not renormalize the mass. Thus, ZrSiS should not be deep in the SM phase. Our proposal is that, the short-range interaction in ZrSiS is not strong enough to turn it into the EI phase, but suffices to drive this material to fall into the intermediate quantum critical region (QCR). In this QCR, the excitonic order parameter has a vanishing mean value and the nodal line fermions remain gapless, in accordance with experiments [38–40]. However, different from SM phase, the quantum fluctuations of excitonic pairs are important in QCR and can substantially renormalize the quasiparticle mass.

To study what could happen if ZrSiS is in the QCR, we carefully treat the interaction between nodal line fermions and excitonic fluctuation by using the renormalization group (RG) approach, and find that the fermion velocities are suppressed, which enhances the effective fermion mass. The quasiparticle residue Z_f decreases rapidly as the energy is lowered, but flows to a small finite value in the zero-energy limit. Thus, ZrSiS is a strongly interacting Fermi liquid near the SM-EI QCP. This explains why the effective mass in ZrSiS is considerably enhanced but does not take a large value.

Model. The action of the free nodal line fermions is

$$S_\psi = \int \frac{d\omega}{2\pi} \frac{d^3\mathbf{k}}{(2\pi)^3} \psi_a^\dagger(\omega, \mathbf{k}) (-i\omega + \mathcal{H}_0(\mathbf{k})) \psi_a(\omega, \mathbf{k}), \quad (1)$$

where Hamiltonian $\mathcal{H}_0(\mathbf{k}) = \frac{(k_\perp^2 - k_F^2)}{2m} \sigma_1 + v_z k_z \sigma_2$ [29, 43]. Here, $k_\perp^2 = k_x^2 + k_y^2$. Near the nodal lines, one can approximate \mathcal{H}_0 by $\mathcal{H}_0 \approx v_F k_r \sigma_1 + v_z k_z \sigma_2$, where $k_r = k_\perp - k_F$, $v_F = k_F/m$ is the fermion velocity within the x - y plane

and v_z is fermion velocity along z -axis. The interaction-induced renormalization of fermion mass can be easily obtained from the renormalization of velocities v_F and v_z . ψ_a is a two component spinor field, and $\sigma_{1,2,3}$ are Pauli matrices. The index $a = 1, 2, \dots, N$ where N is the fermion flavor. In NLSM, the density of states (DOS) behaves as $\rho(\omega) \propto \omega$, which vanishes at the Fermi level, i.e. $\rho(0) = 0$. Notice that, in the simplified two-dimensional model studied in Ref. [34], $\rho(0)$ takes a large finite value. This is because the dispersion of nodal line fermions along z -axis is completely neglected in that model.

\mathcal{H}_0 respects the chiral symmetry: $\{\mathcal{H}_0, \sigma_3\} = 0$. If the fermion acquires a mass term $\mathcal{H}_\Delta = \Delta \sigma_3$ due to excitonic pairing, a finite gap is opened, breaking the chiral symmetry, and the system becomes an EI (amounting to a charge density wave).

The action of excitonic quantum fluctuation, represented by scalar field ϕ , takes the form

$$S_\phi = \int \frac{d\Omega}{2\pi} \frac{d^3\mathbf{q}}{(2\pi)^3} \phi(\Omega, \mathbf{q}) (\Omega^2 + E_b^2 + r) \phi(\Omega, \mathbf{q}), \quad (2)$$

where $E_b^2 = v_{b\perp}^2 q_\perp^2 + v_{bz}^2 q_z^2$. Here, $v_{b\perp}$ and v_{bz} are boson velocities within x - y plane and along z -axis. Boson mass $r \propto (x - x_c)$ measures the distance of the system to SM-EI QCP, and $r = 0$ at QCP. The Yukawa coupling between fermion and boson is described by

$$S_{\psi\phi} = g \int d\tau d^3\mathbf{x} \psi_a^\dagger(\tau, \mathbf{x}) \sigma_3 \psi_a(\tau, \mathbf{x}) \phi(\tau, \mathbf{x}). \quad (3)$$

There is also a ϕ^4 interaction: $S_{\phi^4} = \frac{u}{24} \int d\tau d^3\mathbf{x} \phi^4(\tau, \mathbf{x})$. Here, g and u are coupling coefficients.

Renormalization group results. The model parameters appearing in the total action $S_\psi + S_\phi + S_{\psi\phi} + S_{\phi^4}$ are renormalized by interactions. Their RG equations, derived in the Supplementary Materials, are given by

$$\frac{dv_F}{d\ell} = (C_1 - C_0) v_F, \quad (4)$$

$$\frac{dv_z}{d\ell} = (C_2 - C_0) v_z, \quad (5)$$

$$\frac{dv_{b\perp}}{d\ell} = \frac{1}{2} (C_\perp - C_\phi) v_{b\perp}, \quad (6)$$

$$\frac{dv_{bz}}{d\ell} = \frac{1}{2} (C_z - C_\phi) v_{bz}, \quad (7)$$

$$\frac{dZ_f}{d\ell} = -C_0 Z_f, \quad (8)$$

$$\frac{d\alpha_g}{d\ell} = -(-C_0 + 3C_1 + 2C_3 + C_\phi) \alpha_g, \quad (9)$$

$$\frac{d\beta_g}{d\ell} = (1 - C_\phi - 2C_1 - 2C_3) \beta_g, \quad (10)$$

$$\frac{du}{d\ell} = -\left(C_\perp + \frac{C_z}{2} + \frac{C_\phi}{2}\right) u + \frac{3u^2}{16} + \frac{12\alpha_g\beta_g}{\pi\delta_1\delta_2^2\delta_3}, \quad (11)$$

where ℓ is a running parameter. $\alpha_g = g^2/v_F^3$ is a dimensionless coupling parameter for the Yukawa coupling, and $\beta_g = \frac{Ng^2k_F}{8\pi v_F^2\Lambda}$. We defined three parameters: $\delta_1 = v_z/v_F$,

$\delta_2 = v_{b\perp}/v_F$, and $\delta_3 = v_{bz}/v_F$. The expressions for parameters $C_i \equiv C_i(\alpha_g, \delta_1, \delta_2, \delta_3)$, where $i = 0, 1, 2, 3$, are given in Supplementary Materials. We also define $C_\phi = \beta_g/\delta_1$, $C_\perp = \frac{\beta_g}{4\delta_1\delta_2^2}$, and $C_z = \frac{\beta_g\delta_1}{2\delta_3^2}$. Z_f is the quasiparticle residue: $Z_f \neq 0$ for Fermi liquids and $Z_f = 0$ for non-Fermi liquids.

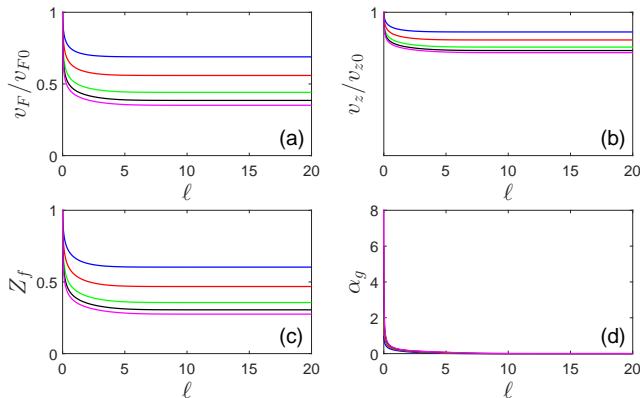


FIG. 2: (a)-(d) Flows of v_F , v_z , Z_f , α_g . Blue, red, green, black, magenta curves represent the initial values $\alpha_{g0} = 1, 2, 4, 6, 8$. The initial conditions $\delta_{10} = 0.1$, $\delta_{20} = 0.05$, $\delta_{30} = 0.05$, and $\beta_{g0} = 0.1$ are used in Figs. 2 and 3.

The energy dependence of model parameters can be obtained by numerically solving the above RG equations. Results are presented in Figs. 2 and 3. For small initial values δ_{10} and δ_{20} , meaning that the motion of boson (excitonic fluctuation) is slower than fermions, we see from Fig. 2(a) that the fermion velocity v_F decreases with lowering energy (growing ℓ), and is saturated to certain finite value v_F^* eventually. According to Fig. 2(a), the ratio v_F^*/v_{F0} can be as small as 0.4 under certain circumstances. Since $v_F = k_F/m$, the ratio between renormalized mass m^* and bare mass m is inversely proportional to v_F^*/v_{F0} . For $\alpha_{g0} = 4$, $m^*/m \approx 2.2$. As a comparison, the quantum oscillation measurements of Pezzini *et al.* [37] revealed that m^*/m is about 2 in the limit of zero magnetic field. From Fig. 2(b), we observe that v_z is also decreased by excitonic fluctuation. Therefore, our RG results clearly show that slow excitonic quantum critical fluctuation could lead to the unconventional fermion mass enhancement observed in ZrSiS [37].

As a system is approaching to a QCP, the renormalized quasiparticle mass m^* may be dramatically enhanced or even diverge [1–7]. In ZrSiS, the ratio $m^*/m \approx 2$. While this turns out to be the largest value ever observed in SM materials [37], it is much smaller than that observed in the aforementioned unconventional superconductors [2–7]. We now explain why m^*/m only takes a moderately large value. From quantum many-body theory, we know that the ratio m^*/m embodies the importance of interparticle interactions. In particular, it is linked to the quasiparticle residue Z_f : $Z_f \sim m/m^*$. For a system tuned to a QCP that exhibits non-Fermi liquid behavior, $Z_f \rightarrow 0$ and m^* diverges. For ZrSiS, we see from Fig. 2(c)

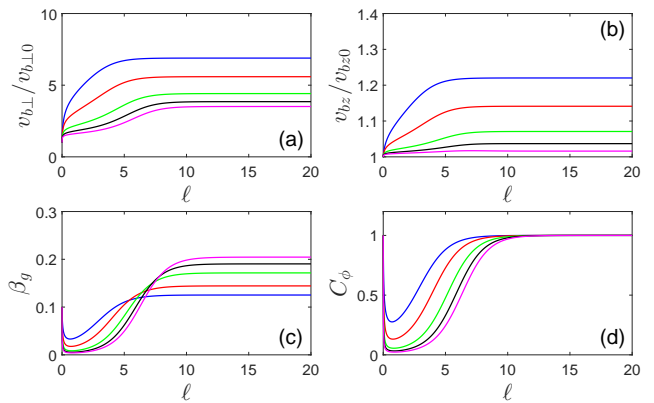


FIG. 3: (a)-(d) Flows of $v_{b\perp}$, v_{bz} , β_g , and C_ϕ , which characterize the impact of Yukawa coupling on the excitonic fluctuation. Blue, red, green, black, magenta curves represent the initial values $\alpha_{g0} = 1, 2, 4, 6, 8$.

that the ℓ -dependence of Z_f is strongly reduced, implying the importance of excitonic fluctuation. However, as ℓ goes to infinity, Z_f does not vanish but flows to a small finite value. On one hand, this result indicates that ZrSiS is still a Fermi liquid, albeit a strongly interacting one. On the other hand, it guarantees that the ratio m^*/m does not take a very large value in ZrSiS. In contrast, the normal states of cuprate, heavy fermion, and iron-based superconductors [1–7] are known to be non-Fermi liquids, thus it is not surprising that their mass enhancement is apparently more significant than ZrSiS.

In the lowest energy limit, the anomalous dimension of fermion field $\eta_\psi = C_0$ vanishes, and the effective strength of Yukawa coupling α_g also flows to zero. Therefore, the excitonic quantum fluctuation is an irrelevant perturbation at low energies. However, before α_g goes to zero, the excitonic fluctuation renormalizes the quasiparticle mass, leading to considerable mass enhancement [37].

The low-energy dynamics of the boson is also affected by the Yukawa coupling. According to Figs. 3(a) and 3(b), $v_{b\perp}$ flows from initial value $v_{b\perp0}$ to a larger constant value $v_{b\perp}^*$, and v_{bz} flows from v_{bz0} to a larger constant v_{bz}^* . Fig. 3(c) shows that β_g approaches to a finite value in the lowest energy limit. Accordingly, C_ϕ , C_\perp , and C_z all flow to finite values. As shown in Fig. 3(d), $C_\phi \rightarrow 1$ in the limit $\ell \rightarrow \infty$. Both C_\perp and C_z flow to unity in the lowest energy limit. The bosonic anomalous dimension η_ϕ is determined by $\eta_\phi = C_\phi^* = 1$.

Roles of LRCI and short-range interactions. There are two types of interactions in NLSMs: LRCI and short-range four-fermion interaction. It is well established that the fermion velocity renormalization unveiled in graphene is produced by the LRCI [21]. This might motivate one to speculate that the mass enhancement of ZrSiS is also due to LRCI [37]. The influence of LRCI on NLSM was studied by Huh *et al.* [43] and Wang and Nandkishore [44], who found that LRCI is irrelevant at low energies. However, whether LRCI increases or reduces velocities

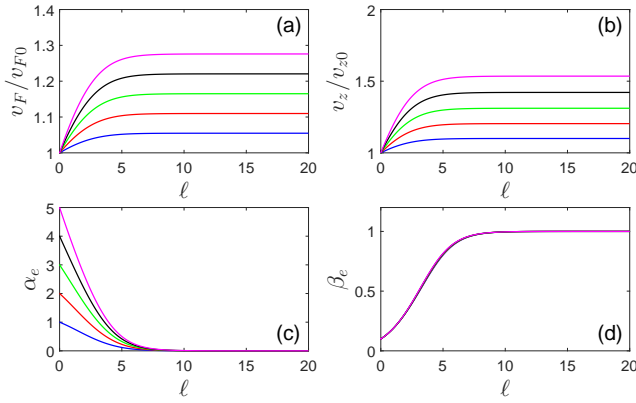


FIG. 4: (a)-(d) Flows of v_F , v_z , α_e , and β_e caused purely by long-range Coulomb interaction. Blue, red, green, black, magenta curves correspond to initial values $\alpha_{e0} = 1, 2, 3, 4, 5$. We choose $\beta_{e0} = 0.1$, $a_0=1$, and $\delta_{10} = 0.2$. Apparently, Coulomb interaction increases velocity v_F and decreases mass.

was not explicitly answered in [43] and [44].

To determine the role played by LRCI, we performed RG analysis of the dynamics of nodal line fermions subjected only to LRCI, with details given in Supplementary Materials. The low-energy behaviors of v_F , v_z , α_e , and β_e are presented in Fig. 4, where $\alpha_e = e^2/v_F$ is the effective strength of LRCI and $\beta_e = \frac{\sqrt{2}e^2k_F}{32\pi\Lambda}$ embodies the dynamical screening. The fermion velocities are always increased by the LRCI. Thus LRCI tends to reduce, rather than enhance, the quasiparticle mass of NLSMs. As shown in Fig. 4(c), the strength parameter α_e flows to zero quickly with growing ℓ , which is consistent with previous work [43, 44]. Since the quasiparticle mass is observed to be clearly enhanced in ZrSiS, we conclude that LRCI plays little role and can be well ignored.

The short-range interactions are important and should be seriously considered [29, 34]. We first emphasize that short-range interaction cannot directly enhance fermion mass as they do not renormalize fermion velocities [29]. However, it can affect fermion mass in an indirect way: strong short-range interaction leads to excitonic pairs of nodal line fermions; this then drives the system to get sufficiently close to SM-EI QCP. Near this QCP, slow excitonic quantum fluctuation enhances the fermion mass.

Observable Quantities. In order to distinguish the QCR from the SM and EI phases, we now calculate a number of observable quantities, including DOS, specific heat, compressibility, and optical conductivities.

Deep in the NLSM phase, the fermion DOS is

$$\rho(\omega) = \frac{Nk_F|\omega|}{2\pi v_F v_z}, \quad (12)$$

and the specific heat depends on temperature as

$$C_v(T) = \frac{9\zeta(3)Nk_F}{\pi v_F v_z} T^2. \quad (13)$$

The compressibility exhibits linear-in- T behavior:

$$\kappa(T) = \frac{2 \ln(2) N k_F}{\pi v_F v_z} T. \quad (14)$$

The optical conductivities within the x - y plane and along the z axis are constants at low energies, namely

$$\sigma_{\perp\perp}(\Omega) = \frac{N e^2 k_F v_F}{32 v_z}, \quad \sigma_{zz}(\Omega) = \frac{N e^2 k_F v_z}{16 v_F}. \quad (15)$$

At the SM-EI QCP, the velocities v_F and v_z are renormalized to smaller values v_F^* and v_z^* by the excitonic fluctuation, which then enhances DOS, specific heat, and compressibility. Our RG results indicate that the ratio v_F^*/v_z^* is smaller than its bare value. Therefore, the optical conductivity is suppressed within x - y plane and is enhanced along z axis near the QCP.

If a finite excitonic gap Δ was generated on the Fermi surface, all the above quantities would be significantly suppressed at low energies. Actually, the DOS becomes

$$\rho(\omega) = \frac{N k_F |\omega|}{2\pi v_F v_z} \theta(|\omega| - \Delta), \quad (16)$$

which is nonzero only above the energy scale set by Δ . The specific heat and compressibility are exponentially reduced by Δ as follows

$$C_v(T) \approx \frac{N k_F}{\pi v_F v_z} \frac{\Delta^4}{T^2} e^{-\frac{\Delta}{T}}, \quad (17)$$

$$\kappa(T) \approx \frac{N k_F}{\pi v_F v_z} \frac{\Delta^2}{T} e^{-\frac{\Delta}{T}}. \quad (18)$$

A discrete chiral symmetry is broken in EI phase, thus there is no Goldstone boson. The specific heat is purely contributed by the fermionic quasiparticles. The optical conductivities vanish at energies below 2Δ :

$$\sigma_{\perp\perp}(\Omega) = \frac{N e^2 k_F v_F}{32 v_z} \left(1 + \frac{4\Delta^2}{|\Omega|^2}\right) \theta(|\Omega| - 2\Delta), \quad (19)$$

$$\sigma_{zz}(\Omega) = \frac{N e^2 k_F v_z}{16 v_F} \left(1 + \frac{4\Delta^2}{|\Omega|^2}\right) \theta(|\Omega| - 2\Delta). \quad (20)$$

In Table I, we list the ω - and T -dependence of observable quantities obtained in the three different regions of phase diagram Fig. 1. By measuring these quantities, one could further verify whether ZrSiS is near or far from the SM-EI QCP.

Summary and Discussion. To summarize, we have studied the behavior of gapless nodal line fermions near the QCP to an EI, and found that the effective fermion mass is considerably enhanced by the excitonic fluctuation. The quasiparticle residue Z_f is substantially suppressed, but flows to a finite value in the lowest energy limit. Thus system should be identified as a strongly correlated Fermi liquid. These results provide a clear explanation of the unconventional mass enhancement in NLSM ZrSiS [37], and indicate that ZrSiS is a rare example of topological SM with intriguing quantum criticality. Similar mass enhancement might also occur in other

TABLE I: Energy or temperature dependence of observable quantities in the SM phase, the EI, and the QCR.

| | $\rho(\omega)$ | $C_v(T)$ | $\kappa(T)$ | $\sigma_{\perp\perp}(\Omega)$ | $\sigma_{zz}(\Omega)$ |
|-----|---|--|--|--|--|
| SM | $ \omega /(v_F v_z)$ | $T^2/(v_F v_z)$ | $T/(v_F v_z)$ | v_F/v_z | v_z/v_F |
| QCR | $ \omega /(v_F^* v_z^*)$ | $T^2/(v_F^* v_z^*)$ | $T/(v_F^* v_z^*)$ | v_F^*/v_z^* | v_z^*/v_F^* |
| EI | $ \omega /(v_F v_z)\theta(\omega - \Delta)$ | $\frac{1}{v_F v_z} \frac{\Delta^4}{T^2} e^{-\frac{\Delta}{T}}$ | $\frac{1}{v_F v_z} \frac{\Delta^2}{T} e^{-\frac{\Delta}{T}}$ | $\frac{v_F}{v_z} \left(1 + \frac{4\Delta^2}{ \Omega ^2}\right) \theta(\Omega - 2\Delta)$ | $\frac{v_z}{v_F} \left(1 + \frac{4\Delta^2}{ \Omega ^2}\right) \theta(\Omega - 2\Delta)$ |

NLSMs so long as the short-range interaction is capable of driving the system sufficiently close to a EI QCP.

The above theoretical analysis is carried out at SM-EI QCP with $r = 0$ and at zero chemical potential $\mu = 0$. In real samples, r and μ are usually not exactly zero. Here we comment on the impact of finite r and finite μ . Finite r weakens the excitonic fluctuation, and thus leads to weaker enhancement of quasiparticle mass. But the enhancement persists for small r . For small μ , theoretical results obtained at $\mu = 0$ are modified only at energy scales below μ . The excitonic fluctuation can still induce striking quantum critical behaviors, including

strong mass enhancement, in the QCR. On the experimental side, previous ARPES measurements on ZrSiS indicated that the Dirac line nodes connect the Dirac points near the Fermi level [39, 40], implying that μ should be quite small. Therefore, we believe that our conclusion is qualitatively reliable for ZrSiS [37].

We acknowledge the support from the National Key R&D Program of China under Grants 2017YFA0403600 and 2016YFA0300404, and that from the National Natural Science Foundation of China under Grants 11574285, 11504379, 11674327, 11974356, U1532267, and U1832209.

-
- [1] H. v. Löhneysen, A. Rosch, M. Vojta, and P. Wölfle, Fermi-liquid instabilities at magnetic quantum phase transitions, *Rev. Mod. Phys.* **79**, 1015 (2007).
- [2] B. J. Ramshaw, S. E. Sebastian, R. D. McDonald, J. Day, B. S. Tan, Z. Zhu, J. B. Betts, R. Liang, D. A. Bonn, W. N. Hardy, and N. Harrison, Quasiparticle mass enhancement approaching optimal doping in a high- T_c superconductor, *Science* **348**, 317 (2015).
- [3] B. Michon, C. Girod, S. Badoux, J. Kačmarčík, Q. Ma, M. Dragomir, H. A. Dabkowska, B. D. Gaulin, J.-S. Zhou, S. Pyon, T. Takayama, H. Takagi, S. Verret, N. Doiron-Leyraud, C. Marcenat, L. Taillefer, and T. Klein, Thermodynamic signatures of quantum criticality in cuprate superconductors, *Nature* **567**, 218 (2019).
- [4] P. Gegenwart, J. Custers, C. Geibel, K. Neumaier, T. Tayama, K. Tenya, O. Trovarelli, and F. Steglich, Magnetic-field induced quantum critical point in YbRh₂Si₂, *Phys. Rev. Lett.* **89**, 056402 (2002).
- [5] Y. Tokiwa, E. D. Bauer, and P. Gegenwart, Zero-field quantum critical point in CeCoIn₅, *Phys. Rev. Lett.* **111**, 107003 (2013).
- [6] P. Aynajian, E. H. da Silva Neto, A. Gyenis, R. E. Baumbach, J. D. Thompson, Z. Fisk, E. D. Bauer, and A. Yazdani, Visualizing heavy fermions emerging in a quantum critical Kondo lattice, *Nature* **486**, 201 (2012).
- [7] P. Walmsley, C. Putzke, L. Malone, I. Guillaumon, D. Vignolles, C. Proust, S. Badoux, A. I. Coldea, M. D. Watson, S. Kasahara, Y. Mizukami, T. Shibauchi, Y. Matsuda, and A. Carrington, Quasiparticle mass enhancement close to the quantum critical point in BaFe₂(As_{1-x}P_x)₂, *Phys. Rev. Lett.* **110**, 257002 (2013).
- [8] C. C. Gu, Z. Y. Zhao, X. L. Chen, M. Lee, E. S. Choi, Y. Y. Han, L. S. Ling, L. Pi, Y. H. Zhang, G. Chen, Z. R. Yang, H. D. Zhou, and X. F. Sun, Field-driven quantum criticality in the spinel magnet ZnCr₂Se₄, *Phys. Rev. Lett.* **120**, 147204 (2018).
- [9] X. Wan, A. M. Turner, A. Vishwanath, and S. Y. Savrasov, Topological semimetal and Fermi-arc surface states in the electronic structure of pyrochlore iridates, *Phys. Rev. B* **83**, 205101 (2011).
- [10] G. Xu, H. Weng, Z. Wang, X. Dai, and Z. Fang, Chern semimetal and the quantized anomalous Hall effect in HgCr₂Se₄, *Phys. Rev. Lett.* **107**, 186806 (2011).
- [11] Z. K. Liu, B. Zhou, Y. Zhang, Z. J. Wang, H. M. Weng, D. Prabhakaran, S.-K. Mo, Z. X. Shen, Z. Fang, X. Dai, Z. Hussain, and Y. L. Chen, Discovery of a three-dimensional topological Dirac semimetal, Na₃Bi, *Science* **343**, 864 (2014).
- [12] B. Yan and C. Felser, Topological materials: Weyl semimetals, *Annu. Rev. Condens. Matter Phys.* **8**, 337 (2017).
- [13] C. Li, C. M. Wang, B. Wan, X. Wan, H.-Z. Lu, and X. C. Xie, Rules for phase shifts of quantum oscillations in topological nodal-line semimetals, *Phys. Rev. Lett.* **120**, 146602 (2018).
- [14] N. P. Armitage, E. J. Mele, and A. Vishwanath, Weyl and Dirac semimetals in three-dimensional solids, *Rev. Mod. Phys.* **90**, 015001 (2018).
- [15] F. Tang, H. C. Po, A. Vishwanath, and X. Wan, Comprehensive search for topological materials using symmetry indicators, *Nature* **566**, 486 (2019).
- [16] T. Zhang, Y. Jiang, Z. Song, H. Huang, Y. He, Z. Fang, H. Weng, and C. Fang, Catalogue of topological electronic materials, *Nature* **566**, 475 (2019).
- [17] M. G. Vergniory, L. Elcoro, C. Felser, N. Regnault, B. A. Bernevig, and Z. Wang, A complete catalogue of high-quality topological materials, *Nature* **566**, 480 (2019).
- [18] J. González, F. Guinea, and M. A. H. Vozmediano, Marginal-Fermi-liquid behavior from two-dimensional Coulomb interaction, *Phys. Rev. B* **59**, R2474(R) (1999).

- [19] V. N. Kotov, B. Uchoa, V. M. Pereira, F. Guinea, and A. H. Castro Neto, Electron-electron interactions in graphene: Current status and perspectives, *Rev. Mod. Phys.* **84**, 1067 (2012).
- [20] J. Hofmann, E. Barnes, and S. Das Sarma, Why does graphene behave as a weakly interacting system?, *Phys. Rev. Lett.* **113**, 105502 (2014).
- [21] D. C. Elias, R. V. Gorbachev, A. S. Mayorov, S. V. Morozov, A. A. Zhukov, P. Blake, L. A. Ponomarenko, I. V. Grigorieva, K. S. Novoselov, F. Guinea, and A. K. Geim, Dirac cones reshaped by interaction effects in suspended graphene, *Nat. Phys.* **7**, 701 (2011).
- [22] P. Goswami and S. Chakravarty, Quantum criticality between topological and band insulators in 3+1 dimensions, *Phys. Rev. Lett.* **107**, 196803 (2011).
- [23] P. Hosur, S. A. Parameswaran, and A. Vishwanath, Charge transport in Weyl semimetals, *Phys. Rev. Lett.* **108**, 046602 (2012).
- [24] E.-G. Moon, C. Xu, Y. B. Kim, and L. Balents, Non-Fermi-liquid and topological states with strong spin-orbit coupling, *Phys. Rev. Lett.* **111**, 206401 (2013).
- [25] H. Isobe, B.-J. Yang, A. Chubukov, J. Schmalian, and N. Nagaosa, Emergent non-Fermi-liquid at the quantum critical point of a topological phase transition in two dimensions, *Phys. Rev. Lett.* **116**, 076803 (2016).
- [26] M. Hirata, K. Ishikawa, K. Miyagawa, M. Tamura, C. Berthier, D. Basko, A. Kobayashi, G. Matsuno, and K. Kanoda, Observation of an anisotropic Dirac cone reshaping and ferrimagnetic spin polarization in an organic conductor, *Nat. Commun.* **7**, 12666 (2016).
- [27] D. Liu, K. Ishikawa, R. Takehara, K. Miyagawa, M. Tamura, K. Kanoda, Insulating Nature of Strongly Correlated Massless Dirac Fermions in an Organic Crystal, *Phys. Rev. Lett.* **116**, 226401 (2016).
- [28] M. Hirata, K. Ishikawa, G. Matsuno, A. Kobayashi, K. Miyagawa, M. Tamura, C. Berthier, and K. Kanoda, Anomalous spin correlations and excitonic instability of interacting 2D Weyl fermions, *Science* **358**, 1403 (2017).
- [29] B. Roy, Interacting nodal-line semimetal: Proximity effect and spontaneous symmetry breaking, *Phys. Rev. B* **96**, 041113(R) (2017).
- [30] L. V. Keldysh and Y. V. Kopayev, Possible instability of semimetallic state toward Coulomb interaction, *Sov. Phys. Solid State* **6**, 2219 (1965).
- [31] J. E. Drut and T. A. Lahde, Is graphene in vacuum an insulator?, *Phys. Rev. Lett.* **102**, 026802 (2009).
- [32] H. Z. Wei, S. P. Chao, and V. Aji, Excitonic phases from Weyl semimetals, *Phys. Rev. Lett.* **109**, 196403 (2012).
- [33] J.-R. Wang, G.-Z. Liu, and C.-J. Zhang, Excitonic pairing and insulating transition in two-dimensional Dirac semimetals, *Phys. Rev. B* **95**, 075129 (2017).
- [34] A. N. Rudenko, E. A. Stepanov, A. I. Lichtenstein, and M. I. Katsnelson, Excitonic instability and pseudogap formation in nodal line semimetal ZrSiS, *Phys. Rev. Lett.* **120**, 216401 (2018).
- [35] B. Roy and M. S. Foster, Quantum multicriticality near the Dirac-semimetal to band-insulator critical point in two dimensions: A controlled ascent from one dimension, *Phys. Rev. X* **8**, 011049 (2018).
- [36] I. F. Herbut and L. Janssen, Topological Mott insulator in three-dimensional systems with quadratic band touching, *Phys. Rev. Lett.* **113**, 106401 (2014).
- [37] S. Pezzini, M. R. van Delft, L. M. Schoop, B. V. Lotsch, A. Carrington, M. I. Katsnelson, N. E. Hussey, and S. Wiedmann, Unconventional mass enhancement around the Dirac nodal loop in ZrSiS, *Nat. Phys.* **14**, 178 (2018).
- [38] L. M. Schoop, M. N. Ali, C. Strasser, A. Topp, A. Varykhalov, D. Marchenko, V. Duppl, S. S. P. Parkin, B. V. Lotsch, C. R. Ast, Dirac cone protected by non-symmorphic symmetry and three-dimensional Dirac line node in ZrSiS, *Nat. Commun.* **7**, 11696 (2016).
- [39] M. Neupane, I. Belopolski, M. M. Hosen, D. S. Sanchez, R. Sankar, M. Szlowska, S.-Y. Xu, K. Dimitri, D. Dhakal, P. Maldonado, P. M. Oppeneer, D. Kaczorowski, F. Chou, M. Z. Hasan, and T. Durakiewicz, Observation of topological nodal fermion semimetal phase in ZrSiS, *Phys. Rev. B* **93**, 201104(R) (2016).
- [40] B.-B. Fu, C.-J. Yi, T.-T. Zhang, M. Caputo, J.-Z. Ma, X. Gao, B. Q. Lv, L.-Y. Kong, Y.-B. Huang, P. Richard, M. Shi, V. N. Strocov, C. Fang, H.-M. Weng, Y.-G. Shi, T. Qian, H. Ding, Dirac nodal surfaces and nodal lines in ZrSiS, *Sci. Adv.* **5**, eaau6459 (2019).
- [41] M. N. Ali, L. M. Schoop, C. Garg, J. M. Lippmann, E. Lara, B. Lotsch, and S. S. P. Parkin, Butterfly magnetoresistance, quasi-2D Dirac Fermi surface and topological phase transition in ZrSiS, *Sci. Adv.* **2**, e1601742 (2016).
- [42] R. Singha, A. K. Pariari, B. Satpati, and P. Mandal, Large nonsaturating magnetoresistance and signature of nondegenerate Dirac nodes in ZrSiS, *Proc. Natl. Acad. Sci. USA* **114**, 2468 (2017).
- [43] Y. Huh, E.-G. Moon, and Y. B. Kim, Long-range Coulomb interaction in nodal-ring semimetals, *Phys. Rev. B* **93**, 035138 (2016).
- [44] Y. Wang and R. M. Nandkishore, Interplay between short-range correlated disorder and Coulomb interaction in nodal-line semimetals, *Phys. Rev. B* **96**, 115130 (2017).

Supplementary Materials for “Quantum Criticality of Excitonic Insulating Transition in Nodal Line Semimetal ZrSiS”

In Section I, we consider the Yukawa-coupling between nodal line fermions and excitonic fluctuation, and present the detailed derivation of the RG equations of various model parameters. In Section II, we consider the long-range Coulomb interaction and derive the RG equations of the corresponding model parameters.

I. INFLUENCE OF QUANTUM FLUCTUATION OF EXCITONIC INSULATING ORDER PARAMETER

A. Propagators

The propagator of free nodal line fermions in the imaginary frequency formalism is given by

$$G_0(\omega, \mathbf{k}) = \frac{1}{-i\omega + A(k_{\perp}^2 - k_F^2)\sigma_1 + v_z k_z \sigma_2}, \quad (21)$$

where $A = 1/(2m)$. In the low-energy regime, the fermion propagator can be written as

$$G_0(\omega, \mathbf{k}) = \frac{1}{-i\omega + v_F k_r \sigma_1 + v_z k_z \sigma_2}, \quad (22)$$

where $v_F = k_F/m$ and $k_r = k_{\perp} - k_F$, and θ is the angle between \mathbf{k}_{\perp} and \mathbf{q}_{\perp} . The bare propagator of boson, which describes the quantum fluctuation of excitonic order parameter, takes the form

$$D_0(\Omega, \mathbf{q}) = \frac{1}{\Omega^2 + v_{b\perp}^2 q_{\perp}^2 + v_{bz}^2 q_z^2}. \quad (23)$$

B. Self-energy of the boson

The self-energy of boson is defined as

$$\Pi(\Omega, \mathbf{q}) = -Ng^2 \int \frac{d\omega}{2\pi} \int' \frac{d^3\mathbf{k}}{(2\pi)^3} \text{Tr} [\sigma_3 G_0(\omega, \mathbf{k}) \sigma_3 G_0(\omega + \Omega, \mathbf{k} + \mathbf{q})]. \quad (24)$$

Substituting Eq. (21) into Eq. (24), we get

$$\Pi(\Omega, \mathbf{q}) = 2Ng^2 \int \frac{d\omega}{2\pi} \int' \frac{d^3\mathbf{k}}{(2\pi)^3} \frac{\omega(\omega + \Omega) + A^2 2k_F k_r (2k_F k_r + 2k_F q_{\perp} \cos(\theta) + q_{\perp}^2) + v_z^2 k_z (k_z + q_z)}{(\omega^2 + E_{\mathbf{k}}^2) [(\omega + \Omega)^2 + A^2 (2k_F k_r + 2k_F q_{\perp} \cos(\theta) + q_{\perp}^2)^2 + v_z^2 (k_z + q_z)^2]}, \quad (25)$$

where $E_{\mathbf{k}} = \sqrt{v_F^2 k_r^2 + v_z^2 k_z^2}$. The prime in \int' means that a proper momentum shell will be chosen in the calculations. Expanding $\Pi(\Omega, \mathbf{q})$ to the quadratic order of Ω , q_r , and q_z , and then performing the integration of ω , we find

$$\begin{aligned} \Pi(\Omega, \mathbf{q}) = & -\Omega^2 N \frac{g^2}{4} \int' \frac{d^3\mathbf{k}}{(2\pi)^3} \frac{1}{E^3(\mathbf{k})} - v_r^2 q_r^2 N \frac{g^2}{2} \int' \frac{d^3\mathbf{k}}{(2\pi)^3} \left[\frac{\cos^2(\theta)}{E^3(\mathbf{k})} - \frac{3v_r^2 k_r^2 \cos^2(\theta)}{2E^5(\mathbf{k})} \right] \\ & - v_z^2 q_z^2 N \frac{g^2}{2} \int' \frac{d^3\mathbf{k}}{(2\pi)^3} \left[\frac{1}{E^3(\mathbf{k})} - \frac{3v_z^2 k_z^2}{2E^5(\mathbf{k})} \right]. \end{aligned} \quad (26)$$

A redefinition $\Pi(\Omega, \mathbf{q}) - \Pi(0, 0) \rightarrow \Pi(\Omega, \mathbf{q})$ has been employed to discard a constant term, such that $\Pi(0, 0) = 0$ is fulfilled. Adopting the relation

$$\int' \frac{d^3\mathbf{k}}{(2\pi)^3} \approx k_F \int' \frac{dk_r dk_z}{(2\pi)^2}, \quad (27)$$

and choosing the following momentum shell

$$b\Lambda < \sqrt{v_F^2 k_r^2 + v_z^2 k_z^2} < \Lambda, \quad (28)$$

where $b = e^{-\ell}$ with ℓ being RG running parameter, we obtain

$$\Pi(\Omega, \mathbf{q}) = -\Omega^2 C_\phi \ell - v_{b\perp}^2 q_\perp^2 C_\perp \ell - v_{bz}^2 q_z^2 C_z \ell, \quad (29)$$

where

$$C_\phi = \frac{Ng^2 k_F}{8\pi v_r v_z \Lambda}, \quad C_\perp = \frac{Ng^2 k_F v_r}{32\pi v_z v_{b\perp}^2 \Lambda}, \quad C_z = \frac{Ng^2 k_F v_z}{16\pi v_r v_{bz}^2 \Lambda}. \quad (30)$$

C. Self-energy of the nodal line fermion

The self-energy of nodal line fermions induced by excitonic fluctuation is

$$\Sigma(\omega, k_F + \mathbf{k}) = g^2 \int' \frac{d\Omega}{2\pi} \frac{d^3 \mathbf{q}}{(2\pi)^3} \sigma_3 G_0(\omega + \Omega, \mathbf{k} + \mathbf{q}) \sigma_3 D_0(\Omega, \mathbf{q}). \quad (31)$$

Here, the momentum vector $\mathbf{k} = (k_x, 0, k_z)$. Substituting Eq. (22) into Eq. (31) gives rise to

$$\Sigma(\omega, k_F + \mathbf{k}) = g^2 \int' \frac{d\Omega}{2\pi} \frac{d^3 \mathbf{q}}{(2\pi)^3} \frac{i(\omega + \Omega) - v_F(k_x + q_x)\sigma_1 - v_z(k_z + q_z)\sigma_2}{(\omega + \Omega)^2 + v_F^2(k_x + q_x)^2 + v_z^2(k_z + q_z)^2} D_0(\Omega, \mathbf{q}). \quad (32)$$

We then expand this function to the leading orders of Ω and \mathbf{k}_i , and insert the expression of $D_0(\Omega, \mathbf{q})$, which yields

$$\begin{aligned} \Sigma(\omega, k_F + \mathbf{k}) &= i\omega \frac{g^2}{16\pi^4} \int' d\Omega dq_x dq_y dq_z \frac{-\Omega^2 + v_F^2 q_x^2 + v_z^2 q_z^2}{(\Omega^2 + v_F^2 q_x^2 + v_z^2 q_z^2)^2} \frac{1}{\Omega^2 + v_{b\perp}^2 (q_x^2 + q_y^2) + v_{bz}^2 q_z^2} \\ &\quad - v_F k_x \sigma_1 \frac{g^2}{16\pi^4} \int' d\Omega dq_x dq_y dq_z \frac{\Omega^2 - v_F^2 q_x^2 + v_z^2 q_z^2}{(\Omega^2 + v_F^2 q_x^2 + v_z^2 q_z^2)^2} \frac{1}{\Omega^2 + v_{b\perp}^2 (q_x^2 + q_y^2) + v_{bz}^2 q_z^2} \\ &\quad - v_z k_z \sigma_2 \frac{g^2}{16\pi^4} \int' d\Omega dq_x dq_y dq_z \frac{\Omega^2 + v_F^2 q_x^2 - v_z^2 q_z^2}{(\Omega^2 + v_F^2 q_x^2 + v_z^2 q_z^2)^2} \frac{1}{\Omega^2 + v_{b\perp}^2 (q_x^2 + q_y^2) + v_{bz}^2 q_z^2}. \end{aligned} \quad (33)$$

Perform integration as follows

$$\int' d\Omega dq_x dq_y dq_z = \left(\int_{b\Lambda}^\Lambda + \int_{-\Lambda}^{-b\Lambda} \right) dq_x \int_{-\infty}^{+\infty} d\Omega \int_{-\infty}^{+\infty} dq_y \int_{-\infty}^{+\infty} dq_z, \quad (34)$$

we obtain

$$\Sigma(\omega, k_F + \mathbf{k}) = i\omega C_0 \ell - v_F k_x \sigma_1 C_1 \ell - v_z k_z \sigma_2 C_2 \ell, \quad (35)$$

where the constants $C_{1,2,3}$ are

$$C_0 = \frac{g^2}{8\pi^3 v_F^3 \delta_2^2} \int_{-\infty}^{+\infty} dx \int_{-\infty}^{+\infty} dy \frac{-x^2 + 1 + \delta_1^2 y^2}{(x^2 + 1 + \delta_1^2 y^2)^2} \frac{1}{\sqrt{\frac{1}{\delta_2^2} x^2 + 1 + \frac{\delta_3^2}{\delta_2^2} y^2}}, \quad (36)$$

$$C_1 = \frac{g^2}{8\pi^3 v_F^3 \delta_2^2} \int_{-\infty}^{+\infty} dx \int_{-\infty}^{+\infty} dy \frac{x^2 - 1 + \delta_1^2 y^2}{(x^2 + 1 + \delta_1^2 y^2)^2} \frac{1}{\sqrt{\frac{1}{\delta_2^2} x^2 + 1 + \frac{\delta_3^2}{\delta_2^2} y^2}}, \quad (37)$$

$$C_2 = \frac{g^2}{8\pi^3 v_F^3 \delta_2^2} \int_{-\infty}^{+\infty} dx \int_{-\infty}^{+\infty} dy \frac{x^2 + 1 - \delta_1^2 y^2}{(x^2 + 1 + \delta_1^2 y^2)^2} \frac{1}{\sqrt{\frac{1}{\delta_2^2} x^2 + 1 + \frac{\delta_3^2}{\delta_2^2} y^2}}, \quad (38)$$

with

$$\delta_1 = \frac{v_z}{v_F}, \quad \delta_2 = \frac{v_{b\perp}}{v_F}, \quad \delta_3 = \frac{v_{bz}}{v_F}. \quad (39)$$

D. Vertex correction to fermion-boson (Yukawa) coupling

The correction to the fermion-boson coupling is

$$\Gamma = g^2 \int' \frac{d\Omega}{2\pi} \frac{d^3\mathbf{q}}{(2\pi)^3} \sigma_3 G_0(\Omega, \mathbf{q}) \sigma_3 G_0(\Omega, \mathbf{q}) \sigma_3 D_0(\Omega, \mathbf{q}). \quad (40)$$

Substituting Eqs. (22) and (23) into Eq. (40), we obtain

$$\Gamma = -\sigma_3 C_3 \ell, \quad (41)$$

where

$$C_3 = \frac{g^2}{8\pi^3 v_F^3 \delta_2^2} \int_{-\infty}^{+\infty} dx \int_{-\infty}^{+\infty} dy \frac{1}{x^2 + 1 + \delta_1^2 y^2} \frac{1}{\sqrt{\frac{1}{\delta_2^2} x^2 + 1 + \frac{\delta_3^2}{\delta_2^2} y^2}}. \quad (42)$$

E. Correction to ϕ^4 coupling

The correction to the ϕ^4 vertex induced by ϕ^4 coupling is

$$\delta u^a = -\frac{3}{2} u^2 \int' \frac{d\Omega}{2\pi} \frac{d^3\mathbf{q}}{(2\pi)^3} D_0(\Omega, \mathbf{q}) D_0(\Omega, \mathbf{q}). \quad (43)$$

Making use of Eq. (23) into Eq. (43), we now re-write δu^a as

$$\delta u^a = -\frac{3u^2}{32\pi^4} \int' d\Omega dq_x dq_y dq_z \frac{1}{(\Omega^2 + v_{b\perp}^2 q_\perp^2 + v_{bz}^2 q_z^2)^2}, \quad (44)$$

which after carrying out integration becomes

$$\delta u^a = -\frac{3u^2}{16\pi^2 v_{b\perp}^3} \frac{\delta_2}{\delta_3} \ell. \quad (45)$$

The correction to ϕ^4 vertex due to the fermion-boson coupling can be computed as follows

$$\begin{aligned} \delta u^b &= 6g^4 N \int' \frac{d^3\mathbf{k}}{(2\pi)^3} \frac{d\omega}{2\pi} \text{Tr} [\sigma_3 G_0(\omega, \mathbf{k}) \sigma_3 G_0(\omega, \mathbf{k}) \sigma_3 G_0(\omega, \mathbf{k}) \sigma_3 G_0(\omega, \mathbf{k})] \\ &= N \frac{3g^4 k_F}{4\pi} \int' dk_r dk_z \frac{1}{(v_F^2 k_r^2 + v_z^2 k_z^2)^{\frac{3}{2}}} \\ &= N \frac{3g^4 k_F}{2v_F v_z \Lambda} \ell. \end{aligned} \quad (46)$$

Now the total correction to ϕ^4 vertex has the form

$$\delta u = \delta u^a + \delta u^b = \left(-\frac{3u^2}{16\pi^2 v_{b\perp}^3} \frac{\delta_2}{\delta_3} + N \frac{3g^4 k_F}{2v_F v_z \Lambda} \right) \ell. \quad (47)$$

F. Derivation of the RG equations

The free action of fermion field ψ is

$$S_\psi = \int \frac{d\omega}{2\pi} \frac{dk_x}{2\pi} \frac{dk_y}{2\pi} \frac{dk_z}{2\pi} \psi_a^\dagger(\omega, \mathbf{k}) \left(-i\omega + \frac{k_x^2 + k_y^2 - k_F^2}{2m} \sigma_x + v_z k_z \sigma_y \right) \psi_a(\omega, \mathbf{k}). \quad (48)$$

In the low-energy regime, this free action can be re-written as

$$S_\psi = k_F \int \frac{d\omega}{2\pi} \frac{dk_r}{2\pi} \frac{dk_z}{2\pi} \psi_a^\dagger(\omega, \mathbf{k}) (-i\omega + v_F k_r \sigma_1 + v_z k_z \sigma_2) \psi_a(\omega, \mathbf{k}). \quad (49)$$

Adding the fermion self-energy to the above free action leads to

$$\begin{aligned} S_\psi &= k_F \int \frac{d\omega}{2\pi} \frac{dk_r}{2\pi} \frac{dk_z}{2\pi} \psi_a^\dagger(\omega, \mathbf{k}) (-i\omega + v_F k_r \sigma_1 + v_z k_z \sigma_2 - \Sigma(\omega, \mathbf{k})) \psi_a(\omega, \mathbf{k}) \\ &= k_F \int \frac{d\omega}{2\pi} \frac{dk_r}{2\pi} \frac{dk_z}{2\pi} \psi_a^\dagger(\omega, \mathbf{k}) (-i\omega e^{C_0\ell} + v_F k_r \sigma_1 e^{C_1\ell} + v_z k_z \sigma_2 e^{C_2\ell}) \psi_a(\omega, \mathbf{k}). \end{aligned} \quad (50)$$

Make the following scaling transformations:

$$\omega = \omega' e^{-\ell}, \quad (51)$$

$$k_r = k'_r e^{-\ell}, \quad (52)$$

$$k_z = k'_z e^{-\ell}, \quad (53)$$

$$\psi = \psi' e^{\frac{(4-C_0)\ell}{2}}, \quad (54)$$

$$v_F = v'_F e^{-(C_1-C_0)\ell}, \quad (55)$$

$$v_z = v'_z e^{-(C_2-C_0)\ell}, \quad (56)$$

and then express the total action in the form

$$S_{\psi'} = k_F \int \frac{d\omega'}{2\pi} \frac{dk'_r}{2\pi} \frac{dk'_z}{2\pi} \psi_a^\dagger(\omega', \mathbf{k}') (-i\omega' + v'_F k'_r \sigma_x + v'_z k'_z \sigma_y) \psi_a(\omega', \mathbf{k}'), \quad (57)$$

which recovers the original form of the fermion action.

The free action of boson field ϕ is given by

$$S_\phi = \int \frac{d\Omega}{2\pi} \frac{dq_x}{2\pi} \frac{dq_y}{2\pi} \frac{dq_z}{2\pi} \phi(\Omega, \mathbf{q}) (\Omega^2 + v_{b\perp}^2 q_\perp^2 + v_{bz}^2 q_z^2) \phi(\Omega, \mathbf{q}). \quad (58)$$

Including the boson self-energy modifies it into

$$\begin{aligned} S_\phi &= \int \frac{d\Omega}{2\pi} \frac{dq_x}{2\pi} \frac{dq_y}{2\pi} \frac{dq_z}{2\pi} \phi(\Omega, \mathbf{q}) (\Omega^2 + v_{b\perp}^2 q_\perp^2 + v_{bz}^2 q_z^2 - \Pi(\Omega, \mathbf{q})) \phi(\Omega, \mathbf{q}) \\ &\approx \int \frac{d\Omega}{2\pi} \frac{dq_x}{2\pi} \frac{dq_y}{2\pi} \frac{dq_z}{2\pi} \phi(\Omega, \mathbf{q}) (\Omega^2 e^{C_\phi\ell} + v_{b\perp}^2 q_\perp^2 e^{C_\perp\ell} + v_{bz}^2 q_z^2 e^{C_z\ell}) \phi(\Omega, \mathbf{q}). \end{aligned} \quad (59)$$

To proceed, we make the following scaling transformations

$$\Omega = \Omega' e^{-\ell}, \quad (60)$$

$$q_x = q'_x e^{-\ell}, \quad (61)$$

$$q_y = q'_y e^{-\ell}, \quad (62)$$

$$q_z = q'_z e^{-\ell}, \quad (63)$$

$$\phi = \phi' e^{\frac{(6-C_\phi)\ell}{2}}, \quad (64)$$

$$v_{b\perp} = v'_{b\perp} e^{-\frac{(C_\perp-C_\phi)\ell}{2}}, \quad (65)$$

$$v_{bz} = v'_{bz} e^{-\frac{(C_z-C_\phi)\ell}{2}}. \quad (66)$$

The modified (by interaction) boson action now has the form

$$S_{\phi'} = \int \frac{d\Omega'}{2\pi} \frac{dq'_x}{2\pi} \frac{dq'_y}{2\pi} \frac{dq'_z}{2\pi} \phi'(\Omega', \mathbf{q}') (\Omega'^2 + v'^2_{b\perp} q'^2_\perp + v'^2_{bz} q'^2_z) \phi'(\Omega', \mathbf{q}'), \quad (67)$$

which has same form as the original action of boson.

The action of the fermion-boson coupling is originally defined as

$$S_{\psi\phi} = g \int \frac{d\omega}{2\pi} \frac{d^3\mathbf{k}}{(2\pi)^3} \frac{d\Omega}{2\pi} \frac{d^3\mathbf{q}}{(2\pi)^3} \psi_a^\dagger(\omega, \mathbf{k}) \sigma_3 \psi_a(\omega + \Omega, \mathbf{k} + \mathbf{q}) \phi(\Omega, \mathbf{q}), \quad (68)$$

which can be further written as

$$S_{\psi\phi} = g k_F \int \frac{d\omega}{2\pi} \frac{dk_r}{2\pi} \frac{dk_z}{2\pi} \frac{d\Omega}{2\pi} \frac{d^3\mathbf{q}}{(2\pi)^3} \psi_a^\dagger(\omega, \mathbf{k}) \sigma_3 \psi_a(\omega + \Omega, \mathbf{k} + \mathbf{q}) \phi(\Omega, \mathbf{q}). \quad (69)$$

This action is changed by the vertex correction to become

$$\begin{aligned} S_{\psi\phi} &= g(1 - C_3\ell) k_F \int \frac{d\omega}{2\pi} \frac{dk_r}{2\pi} \frac{dk_z}{2\pi} \frac{d\Omega}{2\pi} \frac{d^3\mathbf{q}}{(2\pi)^3} \psi_a^\dagger(\omega, \mathbf{k}) \sigma_3 \psi_a(\omega + \Omega, \mathbf{k} + \mathbf{q}) \phi(\Omega, \mathbf{q}) \\ &\approx g e^{-C_3\ell} k_F \int \frac{d\omega}{2\pi} \frac{dk_r}{2\pi} \frac{dk_z}{2\pi} \frac{d\Omega}{2\pi} \frac{d^3\mathbf{q}}{(2\pi)^3} \psi_a^\dagger(\omega, \mathbf{k}) \sigma_3 \psi_a(\omega + \Omega, \mathbf{k} + \mathbf{q}) \phi(\Omega, \mathbf{q}). \end{aligned} \quad (70)$$

Performing the scaling transformations given by Eqs. (51)-(54), and Eqs. (60)-(64), we finally expression the above action as

$$\begin{aligned} S_{\psi'\phi'} &= g k_F e^{-(C_0+C_3+\frac{C_\phi}{2})\ell} \int \frac{d\omega'}{2\pi} \frac{dk'_r}{2\pi} \frac{dk'_z}{2\pi} \frac{d\Omega'}{2\pi} \frac{d^3\mathbf{q}'}{(2\pi)^3} \psi_a'^\dagger(\omega', \mathbf{k}') \sigma_3 \psi_a'(\omega' + \Omega', \mathbf{k}' + \mathbf{q}') \phi'(\Omega', \mathbf{q}') \\ &= g' k_F \int \frac{d\omega'}{2\pi} \frac{dk'_r}{2\pi} \frac{dk'_z}{2\pi} \frac{d\Omega'}{2\pi} \frac{d^3\mathbf{q}'}{(2\pi)^3} \psi_a'^\dagger(\omega', \mathbf{k}') \sigma_3 \psi_a'(\omega' + \Omega', \mathbf{k}' + \mathbf{q}') \phi'(\Omega', \mathbf{q}'), \end{aligned} \quad (71)$$

where the following transformation is made for coupling parameter g :

$$g = g' k e^{(C_0+C_3+\frac{C_\phi}{2})\ell}. \quad (72)$$

The action of ϕ^4 coupling is originally defined as

$$\begin{aligned} S_{\phi^4} &= \frac{u}{24} \int \frac{d\Omega_1}{2\pi} \frac{d^3\mathbf{q}_1}{(2\pi)^3} \frac{d\Omega_2}{2\pi} \frac{d^3\mathbf{q}_2}{(2\pi)^3} \frac{d\Omega_3}{2\pi} \frac{d^3\mathbf{q}_3}{(2\pi)^3} \phi(\Omega_1, \mathbf{q}_1) \phi(\Omega_2, \mathbf{q}_2) \phi(\Omega_3, \mathbf{q}_3) \\ &\quad \times \phi(-\Omega_1 - \Omega_2 - \Omega_3, -\mathbf{q}_1 - \mathbf{q}_2 - \mathbf{q}_3). \end{aligned} \quad (73)$$

The same calculational steps can be repeated to obtain

$$\begin{aligned} S_{\phi'^4} &\approx \frac{1}{24} \left[u - 2C_\phi u \ell + \left(-\frac{3u^2}{16\pi^2 v_{b\perp}^2 v_{bz}} + N \frac{3g^4 k_F}{2v_F v_z \Lambda} \right) \ell \right] \int \frac{d\Omega'_1}{2\pi} \frac{d^3\mathbf{q}'_1}{(2\pi)^3} \frac{d\Omega'_2}{2\pi} \frac{d^3\mathbf{q}'_2}{(2\pi)^3} \frac{d\Omega'_3}{2\pi} \frac{d^3\mathbf{q}'_3}{(2\pi)^3} \phi'(\Omega'_1, \mathbf{q}'_1) \phi'(\Omega'_2, \mathbf{q}'_2) \\ &\quad \times \phi'(\Omega'_3, \mathbf{q}'_3) \phi'(-\Omega'_1 - \Omega'_2 - \Omega'_3, -\mathbf{q}'_1 - \mathbf{q}'_2 - \mathbf{q}'_3). \end{aligned} \quad (74)$$

Redefining the coupling parameter

$$u' = u - 2C_\phi u \ell + \left(-\frac{3u^2}{16\pi^2 v_{b\perp}^2 v_{bz}} + N \frac{3g^4 k_F}{2v_F v_z \Lambda} \right) \ell, \quad (75)$$

we get

$$\begin{aligned} S_{\phi'^4} &\approx u' \int \frac{d\Omega'_1}{2\pi} \frac{d^3\mathbf{q}'_1}{(2\pi)^3} \frac{d\Omega'_2}{2\pi} \frac{d^3\mathbf{q}'_2}{(2\pi)^3} \frac{d\Omega'_3}{2\pi} \frac{d^3\mathbf{q}'_3}{(2\pi)^3} \phi'(\Omega'_1, \mathbf{q}'_1) \phi'(\Omega'_2, \mathbf{q}'_2) \phi'(\Omega'_3, \mathbf{q}'_3) \\ &\quad \times \phi'(-\Omega'_1 - \Omega'_2 - \Omega'_3, -\mathbf{q}'_1 - \mathbf{q}'_2 - \mathbf{q}'_3). \end{aligned} \quad (76)$$

From the transformations of Eqs. (55), (56), (65), (66), (72), (75), we eventually derive the self-consistently coupled

RG equations

$$\frac{dv_F}{d\ell} = (C_1 - C_0) v_F, \quad (77)$$

$$\frac{dv_z}{d\ell} = (C_2 - C_0) v_z, \quad (78)$$

$$\frac{dv_{b\perp}}{d\ell} = \frac{(C_\perp - C_\phi)}{2} v_{b\perp}, \quad (79)$$

$$\frac{dv_{bz}}{d\ell} = \frac{(C_z - C_\phi)}{2} v_{bz}, \quad (80)$$

$$\frac{d\delta_1}{d\ell} = (C_2 - C_1) \delta_1, \quad (81)$$

$$\frac{d\delta_2}{d\ell} = \left(\frac{C_\perp - C_\phi}{2} - C_1 + C_0 \right) \delta_2, \quad (82)$$

$$\frac{d\delta_3}{d\ell} = \left(\frac{C_z - C_\phi}{2} - C_1 + C_0 \right) \delta_3, \quad (83)$$

$$\frac{d\alpha_g}{d\ell} = -(-C_0 + 3C_1 + 2C_3 + C_\phi) \alpha_g, \quad (84)$$

$$\frac{d\beta_g}{d\ell} = (1 - C_\phi - 2C_1 - 2C_3) \beta_g, \quad (85)$$

$$\frac{du}{d\ell} = -\left(C_\perp + \frac{C_z}{2} + \frac{C_\phi}{2} \right) u - \frac{3u^2}{16} + \frac{12\alpha_g\beta_g}{\pi\delta_1\delta_2^2\delta_3}, \quad (86)$$

where

$$\alpha_g = \frac{g^2}{v_F^3}, \quad \beta_g = \frac{Ng^2k_F}{8\pi v_F^2\Lambda}. \quad (87)$$

In the derivation, we have made the redefinition

$$\frac{u}{\pi^2 v_{b\perp}^2 v_{bz}} \rightarrow u. \quad (88)$$

The parameters $C_{0,1,2,3}$, C_ϕ , C_\perp , and C_z appearing in the RG equations are given by

$$C_0 = \frac{\alpha_g}{8\pi^3\delta_2^2} \int_{-\infty}^{+\infty} dx \int_{-\infty}^{+\infty} dy \frac{-x^2 + 1 + \delta_1^2 y^2}{(x^2 + 1 + \delta_1^2 y^2)^2} \frac{1}{\sqrt{\frac{1}{\delta_2^2} x^2 + 1 + \frac{\delta_3^2}{\delta_2^2} y^2}}, \quad (89)$$

$$C_1 = \frac{\alpha_g}{8\pi^3\delta_2^2} \int_{-\infty}^{+\infty} dx \int_{-\infty}^{+\infty} dy \frac{x^2 - 1 + \delta_1^2 y^2}{(x^2 + 1 + \delta_1^2 y^2)^2} \frac{1}{\sqrt{\frac{1}{\delta_2^2} x^2 + 1 + \frac{\delta_3^2}{\delta_2^2} y^2}}, \quad (90)$$

$$C_2 = \frac{\alpha_g}{8\pi^3\delta_2^2} \int_{-\infty}^{+\infty} dx \int_{-\infty}^{+\infty} dy \frac{x^2 + 1 - \delta_1^2 y^2}{(x^2 + 1 + \delta_1^2 y^2)^2} \frac{1}{\sqrt{\frac{1}{\delta_2^2} x^2 + 1 + \frac{\delta_3^2}{\delta_2^2} y^2}}, \quad (91)$$

$$C_3 = \frac{\alpha_g}{8\pi^3\delta_2^2} \int_{-\infty}^{+\infty} dx \int_{-\infty}^{+\infty} dy \frac{1}{x^2 + 1 + \delta_1^2 y^2} \frac{1}{\sqrt{\frac{1}{\delta_2^2} x^2 + 1 + \frac{\delta_3^2}{\delta_2^2} y^2}}, \quad (92)$$

$$C_\phi = \frac{Ng^2k_F}{8\pi v_F v_z \Lambda} = \frac{\beta_g}{\delta_1}, \quad (93)$$

$$C_\perp = \frac{g^2 k_F v_F}{32\pi v_z v_{b\perp}^2 \Lambda} = \frac{\beta_g}{4\delta_1\delta_2^2}, \quad (94)$$

$$C_z = \frac{g^2 k_F v_z}{16\pi v_F v_{bz}^2 \Lambda} = \frac{\beta_g \delta_1}{2\delta_3^2}. \quad (95)$$

The RG flows of fermion velocities v_F and v_z for different initial conditions are shown in Fig. 5. To make our analysis more generic, we let the ratios δ_{20} and δ_{30} to vary within a wide range. We see that, for small values of δ_{20}

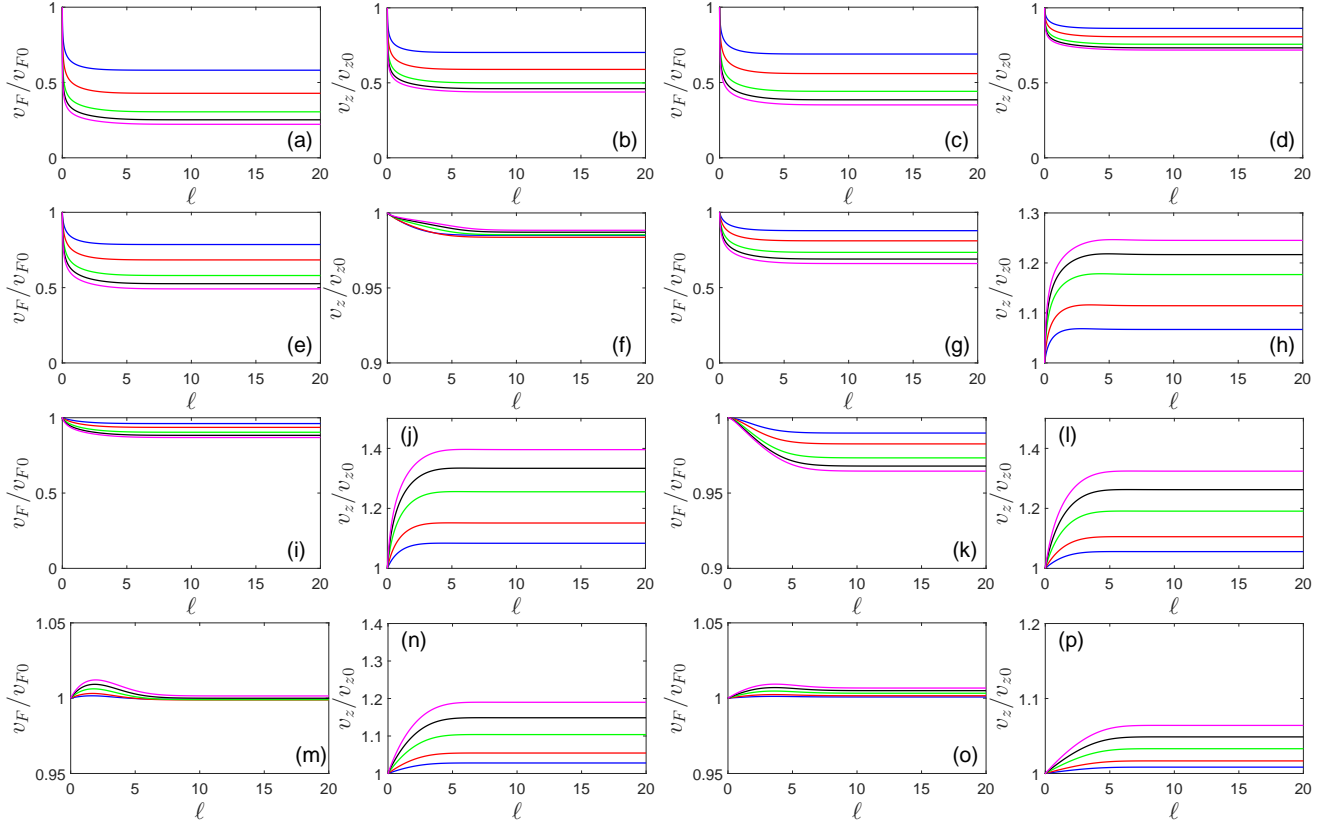


FIG. 5: Flows of v_F and v_z for different initial conditions. (a) and (b): $\delta_{20} = \delta_{30} = 0.02$; (c) and (d): $\delta_{20} = \delta_{30} = 0.05$; (e) and (f): $\delta_{20} = \delta_{30} = 0.1$; (g) and (h): $\delta_{20} = \delta_{30} = 0.2$; (i) and (j): $\delta_{20} = \delta_{30} = 0.5$; (k) and (l): $\delta_{20} = \delta_{30} = 1$; (m) and (n): $\delta_{20} = \delta_{30} = 2$; (o) and (p): $\delta_{20} = \delta_{30} = 5$. Blue, red, green, black, magenta curves represent the initial values $\alpha_{g0} = 1, 2, 4, 6, 8$. The initial conditions $\delta_{10} = 0.1$, $\beta_{g0} = 0.1$ and $u_0 = 1$ are always taken.

and δ_{30} (for simplicity δ_{20} and δ_{30} are assumed to be equal), v_F and v_z are both obviously suppressed. Accordingly, the effective fermion mass is enhanced. However, for sufficiently large values of δ_{20} and δ_{30} , corresponding to the case in which nodal line fermions move more slowly than the boson (excitonic fluctuation), v_F and v_z are slightly increased. Therefore, in order to obtain the observed fermion mass enhancement in ZrSiS, the bare (unrenormalized) velocity of the boson mode (excitonic fluctuation) ought to be smaller than the bare velocity of nodal line fermions.

If the system is in the SM side of the QCP, the parameter r would take a finite value. For finite r , the propagator of boson describing the excitonic fluctuation has the form

$$D_0(\Omega, \mathbf{q}) = \frac{1}{\Omega^2 + v_{b\perp}^2 q_{\perp}^2 + v_{bz}^2 q_z^2 + r}. \quad (96)$$

It is clear that, the excitonic quantum fluctuation is suppressed by finite r , since $D_0(\Omega, \mathbf{q})$ becomes smaller. As r continuously increases from zero, the system is tuned to depart from the QCP into the SM phase. In this process, the mass enhancement is gradually weakened with growing r , and finally disappears at sufficiently large r . As long as the system is not far from the QCP, the quasiparticle mass is always enhanced comparing to the bare mass.

II. INFLUENCE OF LONG-RANGE COULOMB INTERACTION

Here we provide the calculational details of the RG equations caused by long-range Coulomb interaction. The results show that Coulomb interaction tends to reduce the quasiparticle mass, inconsistent with the observed mass enhancement in ZrSiS.

A. Model

The influence of Coulomb interaction on the nodal line fermions can be described by the coupling between the fermion field ψ and a boson field ϕ_e through

$$S_{\psi\phi_e} = ie \int \frac{d\omega}{2\pi} \frac{d^3\mathbf{k}}{(2\pi)^3} \frac{d\Omega}{2\pi} \frac{d^3\mathbf{q}}{(2\pi)^3} \psi^\dagger(\omega, \mathbf{k}) \psi(\omega + \Omega, \mathbf{k} + \mathbf{q}) \phi_e(\Omega, \mathbf{q}), \quad (97)$$

which can be further written as

$$S_{\psi\phi_e} = iek_F \int \frac{d\omega}{2\pi} \frac{dk_r}{2\pi} \frac{dk_z}{2\pi} \frac{d\Omega}{2\pi} \frac{d^3\mathbf{q}}{(2\pi)^3} \psi^\dagger(\omega, \mathbf{k}) \psi(\omega + \Omega, \mathbf{k} + \mathbf{q}) \phi_e(\Omega, \mathbf{q}). \quad (98)$$

The action for the fermion field ψ still can be written as Eq. (49). The action for the boson field ϕ_e takes the form

$$S_{\phi_e} = \int \frac{d\Omega}{2\pi} \frac{dq_x}{2\pi} \frac{dq_y}{2\pi} \frac{dq_z}{2\pi} \phi_e(\Omega, \mathbf{q}) \left(a (q_x^2 + q_y^2) + \frac{1}{a} q_z^2 \right) \phi_e(\Omega, \mathbf{q}). \quad (99)$$

The propagator of boson ϕ_e is given by

$$D_{e0}(\mathbf{q}) = \frac{1}{a (q_x^2 + q_y^2) + \frac{1}{a} q_z^2}. \quad (100)$$

B. The self-energy of boson

The self-energy of boson is defined as

$$\Pi_e(\Omega, \mathbf{q}) = e^2 \int' \frac{d\omega}{2\pi} \frac{d^3\mathbf{k}}{(2\pi)^3} \text{Tr} [G_0(\omega, \mathbf{k}) G_0(\omega + \Omega, \mathbf{k} + \mathbf{q})]. \quad (101)$$

Substituting Eq. (22) into Eq. (101) and expanding to the quadratic order of q_r and q_z , we obtain that the self-energy of boson in the zero energy limit takes the form

$$\Pi_e(\mathbf{q}) = -v_F^2 q_r^2 \frac{e^2}{4} \int' \frac{d^3\mathbf{k}}{(2\pi)^3} \frac{v_z^2 k_z^2}{E_{\mathbf{k}}^5} \cos^2(\theta) - v_z^2 q_z^2 \frac{e^2}{4} \int' \frac{d^3\mathbf{k}}{(2\pi)^3} \frac{v_F^2 k_r^2}{E_{\mathbf{k}}^5}. \quad (102)$$

Carrying out the integration of momenta by adopting the RG scheme shown in Eq. (28), we arrive at

$$\Pi_e(\mathbf{q}) = -C_{e\perp} q_\perp^2 \ell - C_{ez} q_z^2 \ell, \quad (103)$$

where

$$C_{e\perp} = \frac{\beta_e}{\sqrt{2}\delta_1}, \quad C_{ez} = \beta_e \sqrt{2}\delta_1, \quad (104)$$

with

$$\beta_e = \frac{\sqrt{2}e^2 k_F}{32\pi\Lambda}, \quad \delta_1 = \frac{v_z}{v_F}. \quad (105)$$

C. The self-energy of fermions

The self-energy of fermions induced by Coulomb interaction reads as

$$\Sigma_C(\omega, k_F + \mathbf{k}) = -e^2 \int' \frac{d^3\mathbf{q}}{(2\pi)^3} \frac{d\Omega}{2\pi} G_0(\mathbf{k} + \mathbf{q}, i\omega + i\Omega) D_{e0}(\mathbf{q}). \quad (106)$$

Substituting Eqs. (22) and (100) into Eq. (106) and performing the integration of Ω gives rise to

$$\Sigma_C(\omega, k_F + \mathbf{k}) = -\frac{e^2}{2} \int' \frac{d^3\mathbf{q}}{(2\pi)^3} \frac{v_F (k_x + q_x) \sigma_1 + v_z (k_z + q_z) \sigma_2}{\sqrt{v_F^2 (k_x + q_x)^2 + v_z^2 (k_z + q_z)^2}} \frac{1}{a (q_x^2 + q_y^2) + \frac{1}{a} q_z^2}. \quad (107)$$

Expanding to the leading order of \mathbf{k}_i , we obtain

$$\begin{aligned} \Sigma_C(\omega, k_F + \mathbf{k}) &= -v_F k_x \sigma_1 \frac{e^2}{2} \int' \frac{d^3 \mathbf{q}}{(2\pi)^3} \frac{v_z^2 q_z^2}{(v_F^2 q_x^2 + v_z^2 q_z^2)^{\frac{3}{2}}} \frac{1}{a(q_x^2 + q_y^2) + \frac{1}{a} q_z^2} \\ &\quad - v_z k_z \sigma_2 \frac{e^2}{2} \int' \frac{d^3 \mathbf{q}}{(2\pi)^3} \frac{v_F^2 q_x^2}{(v_F^2 q_x^2 + v_z^2 q_z^2)^{\frac{3}{2}}} \frac{1}{a(q_x^2 + q_y^2) + \frac{1}{a} q_z^2}. \end{aligned} \quad (108)$$

Utilizing the RG scheme

$$\int' \frac{d^3 \mathbf{q}}{(2\pi)^3} = \frac{1}{8\pi^3} \left(\int_{b\Lambda}^{\Lambda} + \int_{-\Lambda}^{-b\Lambda} \right) dq_x \int_{-\infty}^{+\infty} dq_y \int_{-\infty}^{+\infty} dq_z, \quad (109)$$

we can get

$$\Sigma_C(\omega, k_F + \mathbf{k}) = -v_F k_x \sigma_x C_{e1} \ell - v_z k_z \sigma_y C_{e2} \ell, \quad (110)$$

where

$$C_{e1} = \frac{\alpha_e}{8\pi^2} F_1(a\delta_1), \quad C_{e2} = \frac{\alpha_e}{8\pi^2} F_2(a\delta_1), \quad (111)$$

with

$$\alpha_e = \frac{e^2}{v_F}, \quad (112)$$

$$F_1(a\delta_1) = \int_{-\infty}^{+\infty} dz \frac{a^2 \delta_1^2 z^2}{(1 + a^2 \delta_1^2 z^2)^{\frac{3}{2}}} \frac{1}{\sqrt{1 + z^2}}, \quad (113)$$

$$F_2(a\delta_1) = \int_{-\infty}^{+\infty} dz \frac{1}{(1 + a^2 \delta_1^2 z^2)^{\frac{3}{2}}} \frac{1}{\sqrt{1 + z^2}}. \quad (114)$$

D. Vertex Correction

The correction for the fermion-boson coupling is defined as

$$\Gamma_e = e^2 \int' \frac{d\Omega}{2\pi} \frac{d^3 \mathbf{q}}{(2\pi)^3} G_0(\Omega, \mathbf{q}) G_0(\Omega, \mathbf{q}) D_{e0}(\mathbf{q}). \quad (115)$$

Substituting Eqs. (22) and (100) into Eq. (115), we find that

$$\Gamma_e = 0. \quad (116)$$

E. Derivation of the RG equations

The free action of ψ is

$$S_\psi = \int \frac{d\omega}{2\pi} \frac{dk_x}{2\pi} \frac{dk_y}{2\pi} \frac{dk_z}{2\pi} \psi^\dagger(\omega, \mathbf{k}) \left(-i\omega + \frac{k_x^2 + k_y^2 - k_F^2}{2m} \sigma_x + v_z k_z \sigma_y \right) \psi(\omega, \mathbf{k}). \quad (117)$$

In the low-energy regime, the free action of ψ can be also written as

$$S_\psi = k_F \int \frac{d\omega}{2\pi} \frac{dk_r}{2\pi} \frac{dk_z}{2\pi} \psi^\dagger(\omega, \mathbf{k}) (-i\omega + v_F k_r \sigma_x + v_z k_z \sigma_y) \psi(\omega, \mathbf{k}). \quad (118)$$

Considering the correction of self-energy of the fermions, the action becomes

$$\begin{aligned} S_\psi &= k_F \int \frac{d\omega}{2\pi} \frac{dk_r}{2\pi} \frac{dk_z}{2\pi} \psi^\dagger(\omega, \mathbf{k}) (-i\omega + v_F k_r \sigma_x + v_z k_z \sigma_y - \Sigma_C(\omega, \mathbf{k})) \psi(\omega, \mathbf{k}) \\ &\approx k_F \int \frac{d\omega}{2\pi} \frac{dk_r}{2\pi} \frac{dk_z}{2\pi} \psi^\dagger(\omega, \mathbf{k}) (-i\omega + v_F k_r \sigma_x e^{C_{e1}\ell} + v_z k_z \sigma_y e^{C_{e2}\ell}) \psi(\omega, \mathbf{k}). \end{aligned} \quad (119)$$

Utilizing the transformations

$$\omega = \omega' e^{-\ell} \quad (120)$$

$$k_r = k'_r e^{-\ell}, \quad (121)$$

$$k_z = k'_z e^{-\ell}, \quad (122)$$

$$\psi = \psi' e^{2\ell}, \quad (123)$$

$$v_F = v'_F e^{-C_{e1}\ell}, \quad (124)$$

$$v_z = v'_z e^{-C_{e2}\ell}, \quad (125)$$

the action becomes

$$S_\psi = k_F \int \frac{d\omega'}{2\pi} \frac{dk'_r}{2\pi} \frac{dk'_z}{2\pi} \psi'^\dagger(\omega', \mathbf{k}') (-i\omega' + v_F k'_r \sigma_x + v_z k'_z \sigma_y) \psi'(\omega', \mathbf{k}'), \quad (126)$$

which recovers the original form of the action.

The free action of the boson field ϕ_e is

$$S_{\phi_e} = \int \frac{d\Omega}{2\pi} \frac{dq_x}{2\pi} \frac{dq_y}{2\pi} \frac{dq_z}{2\pi} \phi_e(\Omega, \mathbf{q}) \left(a (q_x^2 + q_y^2) + \frac{1}{a} q_z^2 \right) \phi_e(\Omega, \mathbf{q}). \quad (127)$$

Including the correction of self-energy of boson, the action of ϕ_e becomes

$$\begin{aligned} S_{\phi_e} &= \int \frac{d\Omega}{2\pi} \frac{dq_x}{2\pi} \frac{dq_y}{2\pi} \frac{dq_z}{2\pi} \phi_e(\Omega, \mathbf{q}) \left(a q_r^2 + \frac{1}{a} q_z^2 - \Pi_e(\mathbf{q}, 0) \right) \phi_e(\Omega, \mathbf{q}) \\ &\approx \int \frac{d\Omega}{2\pi} \frac{dq_x}{2\pi} \frac{dq_y}{2\pi} \frac{dq_z}{2\pi} \phi_e(\Omega, \mathbf{q}) \left(a q_r^2 e^{\frac{C_{e1}}{a}\ell} + \frac{1}{a} q_z^2 e^{aC_{e2}\ell} \right) \phi_e(\Omega, \mathbf{q}). \end{aligned} \quad (128)$$

Using the scaling transformations

$$\Omega = \Omega' e^{-\ell}, \quad (129)$$

$$q_x = q'_x e^{-\ell}, \quad (130)$$

$$q_y = q'_y e^{-\ell}, \quad (131)$$

$$q_z = q'_z e^{-\ell}, \quad (132)$$

$$\phi_e = \phi'_e e^{\left[3 - \frac{1}{4} \left(\frac{C_{e1}}{a} + aC_{e2} \right)\right]\ell}, \quad (133)$$

$$a = a' e^{\left[\frac{1}{2} \left(aC_{e2} - \frac{C_{e1}}{a} \right)\right]\ell}, \quad (134)$$

the action of ϕ'_e becomes

$$S_{\phi'_e} = \int \frac{d\Omega'}{2\pi} \frac{dq'_x}{2\pi} \frac{dq'_y}{2\pi} \frac{dq'_z}{2\pi} \phi'_e(\Omega', \mathbf{q}') \left(a' q_r'^2 + \frac{1}{a'} q_z'^2 \right) \phi'_e(\Omega', \mathbf{q}'), \quad (135)$$

which has the same form as the free action of boson field.

The action of fermion-boson coupling is

$$S_{\psi\phi_e} = ie \int \frac{d\omega}{2\pi} \frac{d^3\mathbf{k}}{(2\pi)^3} \frac{d\Omega}{2\pi} \frac{d^3\mathbf{q}}{(2\pi)^3} \psi^\dagger(\omega, \mathbf{k}) \psi(\omega + \Omega, \mathbf{k} + \mathbf{q}) \phi_e(\Omega, \mathbf{q}). \quad (136)$$

It can be further written as

$$S_{\psi\phi_e} = ik_F \int \frac{d\omega}{2\pi} \frac{dk_r}{2\pi} \frac{dk_z}{2\pi} \frac{d\Omega}{2\pi} \frac{d^3\mathbf{q}}{(2\pi)^3} \psi^\dagger(\omega, \mathbf{k}) \psi(\omega + \Omega, \mathbf{k} + \mathbf{q}) \phi_e(\Omega, \mathbf{q}). \quad (137)$$

Since the vertex correction vanishes, the action still takes the form

$$S_{\psi\phi_e} = ik_F \int \frac{d\omega}{2\pi} \frac{dk_r}{2\pi} \frac{dk_z}{2\pi} \frac{d\Omega}{2\pi} \frac{d^3\mathbf{q}}{(2\pi)^3} \psi^\dagger(\omega, \mathbf{k}) \psi(\omega + \Omega, \mathbf{k} + \mathbf{q}) \phi_e(\Omega, \mathbf{q}). \quad (138)$$

Employing the transformations as shown in Eqs. (120)-(123), and Eqs.(129)-(134), and

$$e' = ee^{-\frac{1}{4}\left(\frac{C_e}{a} + aC_{ez}\right)\ell}, \quad (139)$$

the action becomes

$$S_{\psi'\phi'_e} = ie'k_F \int \frac{d\omega'}{2\pi} \frac{dk'_r}{2\pi} \frac{dk'_z}{2\pi} \frac{d\Omega'}{2\pi} \frac{d^3\mathbf{q}'}{(2\pi)^3} \psi'^{\dagger}(\omega', \mathbf{k}') \psi'(\omega' + \Omega', \mathbf{k}' + \mathbf{q}') \phi'_e(\Omega', \mathbf{q}'), \quad (140)$$

which recovers the form of the original action.

Form Eqs. (124), (125), (134), (139), we get the RG equations

$$\frac{dv_F}{d\ell} = \frac{\alpha}{8\pi^2} F_1(a\delta_1) v_F, \quad (141)$$

$$\frac{dv_z}{d\ell} = \frac{\alpha}{8\pi^2} F_2(a\delta_1) v_z, \quad (142)$$

$$\frac{da}{d\ell} = \frac{\beta_e}{2} \left(\frac{1}{\sqrt{2}a\delta_1} - \sqrt{2}a\delta_1 \right) a, \quad (143)$$

$$\frac{de}{d\ell} = -\frac{\beta_e}{4} \left(\frac{1}{\sqrt{2}a\delta_1} + \sqrt{2}a\delta_1 \right) e, \quad (144)$$

$$\frac{d\alpha}{d\ell} = \left[-\frac{\beta_e}{2} \left(\frac{1}{\sqrt{2}a\delta_1} + \sqrt{2}a\delta_1 \right) - \frac{\alpha}{8\pi^2} F_1(a\delta_1) \right] \alpha, \quad (145)$$

$$\frac{d\beta_e}{d\ell} = \left[1 - \frac{\beta_e}{2} \left(\frac{1}{\sqrt{2}a\delta_1} + \sqrt{2}a\delta_1 \right) \right] \beta_e, \quad (146)$$

$$\frac{d(a\delta_1)}{d\ell} = \left[\frac{\beta_e}{2} \left(\frac{1}{\sqrt{2}a\delta_1} - \sqrt{2}a\delta_1 \right) + \frac{\alpha}{8\pi^2} (F_2(a\delta_1) - F_1(a\delta_1)) \right] a\delta_1. \quad (147)$$

These RG equations are very close to the ones presented in Refs. [43] and [44]. The minor differences result from the fact that a different RG scheme is adopted in our derivation from Refs. [43] and [44].